

Weighing Biinteractions between Fibrin(ogen) and Clot-Binding Peptides Using Microcantilever Sensors

Anna Puiggalí-Jou,^{1,2} Luis J. del Valle,^{1,2} Carlos Alemán,^{1,2} and Maria M.
Pérez-Madrigal^{1,2,*}

¹ *Departament d'Enginyeria Química, ETSEIB, Universitat Politècnica de Catalunya,
Avda. Diagonal 647, Barcelona E-08028, Spain*

² *Center for Research in Nano-Engineering, Universitat Politècnica de Catalunya,
Campus Sud, Edifici C', C/Pasqual i Vila s/n, Barcelona E-08028, Spain*

* m.mar.perez@upc.edu

ABSTRACT

Peptides homing tumor vascularity are considered promising molecular imaging agents for cancer detection at an early stage. In addition to their high binding affinity, improved tissue penetrating ability and low immunogenicity, they can deliver targeted anticancer drugs, thus expanding therapeutic treatments. Among those, the tumor-homing response of CREKA, a linear peptide that specifically binds to clotted-plasma proteins in tumor vessels, has been recently employed to design bioactive systems able to target different cancer types. Within this context, this paper explores the biorecognition event between CR(NMe)EKA, an engineered CREKA-analogue bearing a noncoded amino acid (*N*-methyl-Glu) that is responsible for its enhanced activity, and clotted-plasma proteins (fibrin and fibrinogen) by nanomechanical detection. Specifically, the tumor-homing peptide was covalently attached *via* epoxysilane chemistry onto silicon microcantilever chips that acted as sensors during dynamic mode experiments. Before that, each step of the functionalization process was followed by contact angle measurements, interferometry, X-ray photoelectron spectroscopy, and atomic force microscopy, thus revealing the applied protocol as a suitable strategy. The fibrin(ogen)-binding induced by CR(NMe)EKA was detected by the resonance frequency shift of the cantilevers, and a detection limit of 100 ng/mL was achieved with both proteins. Even though further development is required, this work reflects the promising application of emerging technologies capable of assisting in the fully comprehension of biological interactions and their implications in the biotechnological field.

Keywords: fibrin, fibrinogen, protein binding, tumor-homing peptide, Cys-Arg-Glu-Lys-Ala (CREKA), nanomechanical sensing, microcantilevers

INTRODUCTION

Cancer, which represents the leading cause of morbidity and mortality worldwide (*i.e.* 14 million new cases and 8.2 million cancer related deaths in 2012, the latter year in which information is available [1], requires detection at an early stage to increase the percentage of success of the oncological treatment. Within this context, molecular imaging, which is based on tumor-specific molecular ligands with high binding affinity, plays a central role in cancer detection in conjugation with conventional anatomic clinical imaging techniques (*e.g.* computed x-ray tomography, magnetic resonance imaging, or ultrasound) [2]. Hence, molecular imaging not only provides molecular and physiological information that reveals the presence of cancer in a curable stage, but also it is expected to allow for individualized treatment in real time and drug development [2].

As reviewed by Li and Cho [3], tumor-homing peptides are promising agents to deliver drugs and imaging contrast to tumor sites due to their features [4]: improved tissue penetrating ability (*i.e.* they have a smaller molecular weight - less than 50 amino acids in average - than traditional molecular targeting agents, which include antibodies or their fragments), low immunogenicity, high affinity to targets, as well as stability *in vivo* and easy of handling during synthetic preparation [5-7]. For instance, Arg-Gly-Asp (RGD) and Asn-Gly-Arg (NGR), which are two of the most widely used peptides targeting tumor vascularity (*i.e.* formation of new blood vessels - tumor angiogenesis - during tumor growth and progression), have also been applied to deliver anticancer drugs (*e.g.* chemotherapeutic drugs, cytokines, toxins, nucleic acids, radioactive isotopes, *etc.*) [8-11]. Recently, other novel peptides targeting tumor neovasculature have been reported and tested, such as SVSVGMPKSPRP (SP5-52; several tumor types tested) [12], CGKRRK and CDTRL (HPV16-induced skin carcinoma and breast carcinoma) [13], CKAAKNK (KAA) and CKGAKAR (KAR) (pancreatic tumors) [14], or IFLLWQR (IF7; melanoma and colorectal cancer) [15].

Among those, Cys-Arg-Glu-Lys-Ala (CREKA), which is a linear pentapeptide recognizing clotted plasma proteins in the blood vessels and stroma of tumors [16], was identified using *in vivo* screening of phage-display peptide libraries [13-17] and has been the focus of recent studies [18,19]. Although the exact site of binding remains unknown, evidence strongly suggests that CREKA interacts with fibrin-fibronectin complexes present in tumor vessels [19]. CREKA has targeted different tumor types

(*i.e.* prostate cancer, gliomas, and lung cancer) [20-22], and it has also induced tumor clotting, thus creating further binding sites in a self-amplifying effect [20]. However, as stated by Stefanelli and Baker [23], CREKA's specific binding affinity has not been reported yet.

Furthermore, a combination of simulated annealing and molecular dynamics have revealed CREKA's energy landscape and bioactive conformation (*i.e.* a turn-like structure in which the charged groups of Arg, Glu, and Lys form stable intermolecular interactions) [24,25], thus allowing for the design of CREKA-based peptides with enhanced features [26]. Specifically, by substituting Glu with its *N*-methyl derivative (*N*-methyl-Glu), Agemy *et al.* prepared an analogue, CR(*N*Me)EKA, that displayed better tumor-homing response than CREKA [20]. Therefore, taking advantage of such behavior, in recent works, we have prepared bioactive platforms by combining poly(3,4-ethylenedioxythiophene) (PEDOT), a conducting polymer featuring superior electrochemical properties, with either CREKA [27] or CR(*N*Me)EKA [28]. The excellent electrochemical properties displayed by PEDOT were retained when combined with CREKA and even improved when using the *N*-methyl variant. Moreover, the presence of *N*-methyl-Glu was found to modify the biocomposite-fibrin interactions, being fibrin-coated PEDOT-CR(*N*Me)EKA able to promote the adhesion of tumor cells.

During the last years, the application of nanomechanical sensing for biological purposes[29] has increased considerably, as the review by Calleja *et al.* clearly evidences [30]. Briefly, this technology is based on the microcantilever mechanical response after interacting with a biological analyte, either as a deformation-bending (static mode) or a resonance frequency shift (dynamic mode) [31]. However, despite the fact that this biodetection tool is still far from being a practical alternative to other well established bioanalytical techniques (*e.g.* ELISA, microarrays and electrophoresis methods), nanomechanical sensors display other advantages (*e.g.* manageability, easy of synthesis and functionalization, and high intrinsic sensitivity) [32], that make them suitable for specific biomedical purposes: drug detection [33], quantification of biological agents [34,35], as well as understanding biological interactions [36], and detecting bacterial resistance to antibiotics [37]. For example, Kosaka *et al.* detected ultralow concentrations (*i.e.* ranging from 10 ag/mL to 1 pg/mL in undiluted serum) of two low-abundant cancer biomarkers using microcantilevers as nanomechanical transducers in sandwich bioassays labelled with gold nanoparticles (Np) [34].

Similarly, highly crystalline TiO₂ shells on magnetic cores were applied onto microcantilever sensors to detect very low concentrations (0.1 pg/mL) of multiple protein biomarkers in human serum [35]. Additionally, nanomechanical sensors achieve lower limits of detection than those obtained with other commonly used non-labeled techniques, such as surface plasmon resonance (SPR) or quartz crystal microbalance (QCM) [38].

Within this context, and considering that CREKA-based biocomposites behave as excellent candidates to be applied for biomedical purposes, it seems of major importance to make an effort in understanding the biological interactions that the tumor-homing peptide CR(*N*Me)EKA establishes. Accordingly, this work aims on detecting biomolecular recognition events between CR(*N*Me)EKA-functionalized microcantilever arrays and fibrin (Fb), fibrinogen (Fg), or bovine serum albumin (BSA) by means of nanomechanical sensing and, if possibly, quantitatively determine the detection limit. The modified pentapeptide has been covalently attached to Si surfaces *via* epoxysilane chemistry. Thus, to ensure an efficient surface immobilization, each step of the functionalization process has been characterized by contact angle (CA), interferometry, X-ray photoelectron spectroscopy (XPS), and atomic force microscopy (AFM). Finally, dynamic mode tests evidence changes in the resonance frequency of the cantilevers according to the adsorbed mass.

EXPERIMENTAL SECTION

Materials

Single side polished Si wafers (3 in. diam. × 0.5 mm thickness, <100>, N-type, crystalline with a cubic lattice of $a = 5.4037 \text{ \AA}$) were purchased from Sigma-Aldrich, while Octosensis Microcantilever-Arrays (chips with 8 mono crystalline Si cantilevers, 500 μm in length) were obtained from Micromotive GmbH (Mainz, Germany). CREKA and CR(*N*Me)EKA peptides with > 98% of HPLC purity were purchased from Biomatik (Toronto, ON). The following chemicals were purchased from Sigma-Aldrich and used as received without further purification: isopropanol, (3-glycidyloxypropyl)trimethoxysilane (98%, SigmaAldrich), toluene (99.8%), *N*^α,*N*^α-bis(carboxymethyl)-L-lysine hydrate (TLC) (97%), 1-[(3-dimethylamino)propyl]-3-ethylcarbodiimide methiodide (EDC), *N*-hydroxysuccinimide (NHS), 2-(*N*-

morpholino)ethanesulfonic acid (MES), 2-amino-2-(hydroxymethyl)-1,3-propanediol (Tris base), 3,3',5,5'-tetramethylbenzidine (TMB) ($\geq 99\%$), carbonate/bicarbonate buffer, phosphate buffered saline (PBS, pH 7.4), bovine serum albumin (BSA, lyophilized powder, crystallized, $\geq 98.0\%$), Tween® 20, and Fg and Fb from human plasma. Sodium chloride was purchased from Panreac (Spain). Finally, the primary (anti-Fib/Fg, mouse monoclonal IgM, MFB-HB) and the conjugate antibodies (anti-Mouse IgM secondary ab, HRP conjugated, Goat IgG polyclonal) used in ELISA tests were purchased from ThermoFisher Scientific.

Silicon functionalization

The functionalization protocol, which was applied to Si substrates (either Si pieces or microcantilever chips) was composed of different steps:

- 1) *Cleaning*. Si disks were cut into $0.5 \times 0.5 \text{ cm}^2$ pieces. Before being functionalized, Si pieces and microcantilevers were activated by UV/ozone treatment. Specifically, samples were washed 3 times (5 min each) with isopropanol and placed in a UVO-Cleaner (model 42-220, Jelight Company, Inc., Irvine, CA, USA) for 30 min. Samples were stored under vacuum.
- 2) *Silanization*. Activated samples were silanized with 0.2% solution of (3-glycidyloxypropyl)trimethoxysilane in dry toluene overnight at room temperature under nitrogen atmosphere. Afterwards, samples were washed with toluene and milli-Q water. Then, they were incubated into 100 mM TLC solution in 50 mM carbonate buffer (pH 9.5) overnight at room temperature under gentle agitation. Later, Si substrates were washed with 50 mM carbonate buffer pH 9.5 and milli-Q water.
- 3) *Activation*. Samples were further modified by the reaction of the carboxyl groups at the Si surface with a mixture of 100 mM EDC and 150 mM NHS, both dissolved in 10 mM MES (pH 5.5). Samples were incubated for 30 minutes at 37 °C under gentle agitation and then extensively rinsed with 10 mM MES.
- 4) *Immobilization of the pentapeptide*. A solution of 100 $\mu\text{g}/\text{mL}$ of CREKA or CR(NMe)EKA were prepared in 10 mM MES (pH 5.5). The cantilevers/Si pieces were incubated for 2 hours at 37 °C. After that, the samples were washed with 10 mM MES (pH 5.5) and incubated for 45 minutes at 37 °C with 1 \times PBS with 0.3 M NaCl in order to desorb those peptide fragments not covalently bonded to the

surface. The surface of the cantilever/Si pieces was subsequently blocked to prevent nonspecific interactions by dipping the substrates into a 1 mg/mL BSA solution in 10 mM MES with 0.05% Tween® 20 (pH 5.5) for 1 hour at room temperature with gentle agitation. Thereafter, samples were washed using MES pH 5.5 with 0.05% Tween 20 (pH 5.5).

5) *Protein recognition.* The blocked surfaces were incubated in Fg or Fb solutions (PBS with 0.05% Tween® 20 at pH 7.4) with varying protein concentration (0, 50, 100, 500, and 10000 ng/mL). Fibrin, which is an insoluble powder, was firstly dissolved in 1 N NaOH at 1 mg/mL. Subsequently, this solution was further diluted with PBS (0.05% Tween® 20 at pH 7.4) to obtain all the aliquots. After the incubation time (1 hour, 37 °C), samples were washed with PBS + 0.05% Tween® 20, PBS, and water, and were finally dried at room temperature.

Wettability

Contact angle (CA) measurements were conducted using the water drop method. 0.5 µL of milliQ water drops were deposited onto the Si surface and recorded after stabilization with the equipment OCA 15EC (DataPhysics Instruments GmbH, Filderstadt). The SCA20 software was used to measure the CA, which is shown here as the average of at least 30 measures for each condition.

X-ray photoelectron spectroscopy (XPS)

XPS was used to analyze the chemical composition of Si surfaces. The system (SPEC Surface Nano Analysis GmbH, Berlin, Germany) was equipped with a non-monochromatic twin anode X-ray source XR50 of Mg/Al (1253 eV/1487 eV). Specifically, the Al anode was operated at 150 W. Detector pass energy was set at 25 eV and 0.1 eV for the survey and the narrow scans (high resolution spectra), respectively, at a pressure below 7.5×10^{-9} mbar. Casa XPS software (Version 2.3.16, Casa Software Ltd., Teignmouth, UK) was used to fit and perform peak integration of spectra. The C 1s peak was used as an internal reference (284.8 eV). High resolution XPS spectra were acquired by Gaussian–Lorentzian curve fitting after S-shape background subtraction.

Interferometry

Green light interferometry in vertical scanning interferometry mode (Wyko NT9300 Optical Profiler, Veeco Instruments, New York, NY, USA) was used to evaluate the roughness of Si pieces after each functionalization step. The mean root square roughness (Rq), which is the average height deviation taken from the mean data plane, was measured in five randomly chosen areas ($25 \times 25 \mu\text{m}^2$) of three replicates for each step.

Atomic Force Microscopy (AFM)

AFM was conducted to obtain topographic images of the functionalized surfaces using Si TAP 150-G probes (Budget Sensors, Bulgaria) with a frequency of 150 kHz and a force constant of 5 N/m. Images were obtained with an AFM Dimension microscope using a NanoScope IV controller under ambient conditions in tapping mode. The row scanning frequency was set between 0.6 and 0.8 Hz. The Rq was determined using the statistical application of the NanoScope Analysis software (1.20, Veeco).

Protein binding affinity (ELISA)

Si wafers ($0.5 \times 0.5 \text{ cm}^2$) were deposited into a standard 96 well-plate. The coating protein (BSA, Fg, or Fb) was diluted to a concentration of 1 $\mu\text{g/mL}$ within the coating buffer (0.2 M bicarbonate buffer pH 9.4) and added (100 μL per well) on the plate. The 96-well plate was incubated overnight at 4 °C for 1 hour at 37 °C. Later, the plate was washed 3 times (5 minutes each) with 200 μL of the washing buffer (25 mM Tris, 0.15 M NaCl, 0.05% Tween 20 pH 7.2). Then, 300 μL of the blocking buffer (2 % BSA in washing buffer) were added to each well. The plate was covered and incubated at room temperature for 1 hour or overnight at 4 °C. The blocker was removed, and 200 μL of the primary antibody (Anti-Fib/Fg, mouse monoclonal IgM, MFB-HB) (1:1000) were added to each well. The plate was covered and incubated at room temperature for 1 hour. Afterwards, the plate was washed 3 times (5 minutes each) with the washing buffer (200 μL). The conjugated antibody (Anti-Mouse IgM secondary ab, HRP conjugated, Goat IgG polyclonal) (1:50000) was added to each well (200 μL). Again, the plate was covered and incubated at room temperature for 1 hour. The plate was washed 6 times (5 minutes each) with the washing buffer (200 μL). The substrate 3,3',5,5'-tetramethylbenzidine (TMB) was allowed to equilibrate at room temperature before use and was protected from light. Finally, after removing the washing buffer, 100

μL of TMB were added. The color of the solution slowly developed to 650 nm; after 15 min at 37 °C the plate was read.

Statistical analysis

All the experiments were performed in triplicate. Statistical comparison of values was based on a 2-way ANOVA using Tukey's test for pair-wise comparison with $p < 0.05$.

Nanomechanical biosensing: resonance frequency measurements

Monocrystalline Si microcantilever chips containing arrays of 8 cantilevers (Micromotive GmbH) were used for the nanomechanical biosensing measurements. Specifically, the nominal length, width, and thickness of the cantilevers were 500, 90 ± 2 and 1 μm , respectively. The fundamental resonance frequency is 5205.6 ± 161.7 kHz, obtained after averaging the response of 65 cantilevers. Resonance frequency measurements were conducted less than 24 hours after the protein (BSA, Fg, or Fb) recognition event onto the cantilever surface in a nitrogen atmosphere at 25 °C. Figure 1 illustrates the experimental setup. Hence, added mass onto the cantilever induces a shift in the resonance frequency that can be quantitatively measured by either an optomechanical or an electromechanical transduction scheme. In this case, SCALA (Scanning Laser Analyzer) is the optical read-out technology used during testing (Mecwins S.L., Spain) [39,40]. This platform is based on the automated two-dimensional scanning of a single laser (1 mW) beam by voice-coil actuators perpendicularly located. Displacements over a range of several millimeters at speeds up to 10 mm/s and with an accuracy of 100 nm are achieved. Once the laser beam is reflected by the cantilever array, the exact position and intensity of the reflected spot is collected by a two-dimensional linear position detector (PSD). Moreover, TRACKER, which is an algorithm that recognizes reflected intensity patterns, locates cantilever sensors in a fully automated process.

RESULTS AND DISCUSSION

CREKA and CR(NMe)EKA, which are the tumor-homing pentapeptides used in this work, are displayed in Scheme 1. Both biomolecules bind to clotted plasma proteins overexpressed in cancerous tissue (tumor stroma and the walls of vessels) [41]. Briefly, plasma proteins, such as Fg, which is the Fb precursor, and fibronectin, another protein

crosslinked to Fb during blood clotting, leak from tumor vessels (*i.e.* they are more fragile and irregular than normal vasculature), thus being converted to Fb by procoagulant factors, which are commonly found in tumor environments [41]. Hence, the Fb meshwork localized in the interstitial spaces of tumors acts as CREKA's binding sites for effective tumor imaging or drug delivery.

The tumor-homing response of CREKA was enhanced by protecting the pentapeptide against proteolytic degradation [20]. Specifically, several *N*- and *C*^α-methylated amino acids were replaced without inducing changes in the peptide conformational profile. Among them, CR(*N*Me)EKA (Glu residue modified, Scheme 1) was reported to be significantly more active than CREKA while displaying greater stability. Although both pentapeptides accumulate in areas rich in Fb and Fg, CR(*N*Me)EKA is chosen as the tumor-specific molecular ligand in this work for nanomechanical biosensing experiments. However, during the optimization and characterization of the functionalization protocol, CREKA is used as control to verify any variation provoked by the presence of the *N*Me-Glu residue.

CREKA/CR(*N*Me)EKA silicon surface functionalization

Before immobilizing CR(*N*Me)EKA onto the surface of chips used for nanomechanical biosensing, the reliability and efficiency of the functionalization protocol was confirmed by using bare Si substrates ($0.5 \times 0.5 \text{ cm}^2$) as control test surface. Figure 2 depicts the functionalization protocol followed to bind CR(*N*Me)EKA onto Si surfaces. The pentapeptide was covalently bonded to the surface by following a previously reported silanization process [42]. Although this approach requires more steps than other procedures (*i.e.* physical adsorption of the biomolecule onto the surface), it results in an irreversible and more stable binding.

As it can be observed in Figure 2, after generating hydroxyl groups by UV/ozone exposure (all physisorbed contamination is removed prior modification), silanization was conducted with (3-glycidyloxypropyl)trimethoxysilane. In the next step, TLC enriched the surface with carboxyl groups that were activated by EDC/NHS. Finally, CR(*N*Me)EKA was covalently attached to the surface by the amide bonds created between activated carboxylates and the amino groups from the pentapeptide. It should be noted that, as the sulfhydryl group of the single Cys residue is not required for binding, this strategy allows for coupling the pentapeptide to other moieties, such as

anticancer drugs or fluorescent dyes. Accordingly, this procedure can add multifunctionality to CREKA-tethered systems if required in a biomedical context.

As an initial indicator of the satisfactory evolution of the functionalization process, Figure 3a displays the variation in the wettability of the Si surface according to each step of the protocol previously described. Hence, $-OH$ groups generated due to the UV/ozone treatment notably decrease the CA value of bare Si from $92.7^\circ \pm 5.0^\circ$ to $30.0^\circ \pm 5.0^\circ$, indicating the formation of a highly hydrophilic surface. This observation can be ascribed to both the removing of hydrophobic substances from the Si surface, as well as the newly formed hydroxyl groups. In contrast, hydrophobic epoxysilane-coated surfaces show a CA value of $59.8^\circ \pm 2.8^\circ$, which decreases to $34.4^\circ \pm 3.3^\circ$ in the next step because of $-COOH$ groups provided by TLC. The final step of the functionalization process induces a slight increase in the surface hydrophobicity regardless the pentapeptide used, CREKA ($51.9^\circ \pm 3.9^\circ$) or CR(NMe)EKA ($49.4^\circ \pm 4.5^\circ$).

Although CA results are in good agreement with the expected chemical composition of each functionalization step, the functionalization protocol was corroborated by XPS. Table 1 summarizes the atomic percentage composition and N/C, N/O, and N/Si atomic ratio values of the surfaces throughout each step of the functionalization process. As expected, the composition of control Si-OH surfaces accounts for O 1s (47.7%) and Si 2p (38.9%), with the percentage of C 1s (13.4%) ascribed to atmospheric contamination. In good agreement with CA values, the UV/ozone treatment is responsible for the high percentage of O 1s signal ($O/Si = 1.19$ and $O/C = 3.56$). In the next two functionalization steps, epoxysilane and TLC are bonded to Si-OH surfaces. Consequently, the O/C ratio decreases to 1.71 and 1.46, respectively. However, although the content of N 1s is not altered by the incorporation of TLC, the CA value of the surface ($34.4^\circ \pm 3.3^\circ$) confirms the presence of TLC. Finally, the adequate covalent binding of the two pentapeptides onto the Si substrates is detected not only by the increase in the N 1s content to 2% and 2.3% for CREKA and CR(NMe)EKA, respectively, but also by the reduction in the atomic percentage of Si 2p as well as the increase in C 1s content. The high resolution spectra of N 1s (Figure 4) confirm the peptide attachment since the deconvolution of the signal led to three well-defined peaks. The central peak, which is located at *ca.* 400 eV, corresponds to the amide bonds of the peptide backbone (N-C=O-), whereas the other two peaks at ~ 398 eV and ~ 401 eV are

attributed to the amino groups ($-\text{NH}_2$) and free protonated amino groups (NH_3^+), respectively, present in the side chain groups of CREKA and CR(NMe)EKA [43].

Finally, the topography of the modified surfaces (scanned areas of $5 \times 5 \mu\text{m}^2$) was observed by AFM to monitor each step of the functionalization process. Figure 5 displays height and phase images of Si-OH and CR(NMe)EKA-functionalized surfaces, whereas the results for the intermediate steps (*i.e.* epoxysilane and TLC) and CREKA-functionalized surfaces are included in Figure S1. Upon coating with the pentapeptide (Figure 5), the smooth and homogenous features of Si-OH ($R_q = 0.4 \text{ nm}$) evolves towards a rougher surface, even though the R_q values of the modified interfaces are still small (in the range between 0.4 nm and 1 nm). Moreover, AFM phase images, which register phase signal shifts due to changes in the adhesion force between the tip and the surface (*i.e.* stiffness/softness), allow for the chemical mapping of the surface. Specifically, no phase contrast is observed for any step of the functionalization process, thus verifying the complete coverage of the Si substrate, which is in good agreement with the XPS results.

Aware that R_q values depend on the analyzed area, interferometric measurements were also conducted to determine such parameter but considering bigger scanned areas ($25 \times 25 \mu\text{m}^2$). As it is depicted in Figure 3b, the UV/ozone treatment did not alter the topography of the Si surface (*i.e.* R_q values for Si and Si-OH surfaces are $0.9 \pm 0.3 \text{ nm}$ and $1.0 \pm 0.4 \text{ nm}$, respectively). As described previously, R_q increases after each step of the functionalization process. Thus, with respect to Si-OH, there is an increment in roughness of 120%, 239%, 305%, and 312% for epoxysilane ($2.3 \pm 0.5 \text{ nm}$), TLC ($3.5 \pm 0.9 \text{ nm}$), CREKA ($4.2 \pm 0.3 \text{ nm}$), and CR(NMe)EKA ($4.3 \pm 1.6 \text{ nm}$), respectively.

Overall, the findings derived from CA measurements, topographical characterization, and, most importantly, chemical composition analyses, confirm the proper covalent attachment of CREKA and CR(NMe)EKA onto Si surfaces. Hence, the suitability of the described functionalization protocol, which is based on a silanization process, has been proven, and thus can be applied to microcantilever Si chips for the following nanomechanical experiments.

CREKA and CR(NMe)EKA binding affinity

Before analyzing the interactions between CR(NMe)EKA pentapeptide and Fb or Fg by means of nanomechanical characterization, ELISA binding assays were conducted to verify such biorecognition event. In this case, we approached the experiment

qualitatively, our focus being whether CREKA- and CR(NMe)EKA-functionalized Si surfaces still recognize clotted plasma.

Figure 6 depicts the binding affinity of CREKA and CR(NMe)EKA-functionalized Si surfaces towards Fb, Fg, or BSA as the absorbance at 650 nm in PBS media. Tissue culture polystyrene (TCP) and Si–OH surfaces were used as control substrates. As it can be seen, in PBS, the Fb- and Fg-binding capability of CR(NMe)EKA-functionalized Si surfaces is 118% and 174% higher, respectively, than that displayed by CREKA-functionalized substrates. Besides, no BSA interaction occurred, thus further confirming the biorecognition of this tumor-homing peptide for Fb and Fg complexes. The overall of these results corroborate the role played by NMe-Glu in Fb/Fg interaction [20]. More specifically, such residue is crucial to promote the protein binding mechanism, either by enhancing the activity of the tumor-homing peptide or improving its stability. In addition, the binding site of CR(NMe)EKA is not altered by the functionalization protocol. Accordingly, on the light of these results and considering our previous works [27,28], we selected CR(NMe)EKA as the molecular ligand for nanomechanical biosensing tests.

Nanomechanical biosensing: Resonance frequency measurements

The microcantilever-based biosensing emerging technology has been applied in this work to observe and analyze the binding affinity of CR(NMe)EKA towards Fb and Fg proteins. Among other features, this platform is characterized by high sensitivity, label-free detection, and small sample consumption due to the size of the microcantilevers (*ca.* 1000 μm^2) [44].

Specifically, CR(NMe)EKA-functionalized Si chips containing arrays of 8 cantilevers (Figure S2), thus using various sensors in parallel, were operated in the dynamic mode combining a scanning laser, the beam deflection method, piezoelectrical excitation (an actuator is located beneath the chip base) and analysis of the first vibration mode [45]. After being cleaned (*i.e.* isopropanol + 30' UV/ozone exposure), these commercial chips - 500 μm long, ~100 μm wide, and 1 μm thick - exhibited a fundamental resonance frequency of 5205.6 ± 161.7 kHz ($n = 65$) measured in a N_2 atmosphere at 25 °C. The eigenmode shape obtained during frequency excitation is plotted for a representative cleaned chip in Figure S3.

In general, the results take into consideration the response of at least 10 cantilevers at each concentration. Besides, data for the Fb-binding event was collected in two

independent experiments. Figure 7a plots the resonance frequency shift of microcantilevers incubated in the presence of Fb, Fg, or BSA at a concentration of 10 $\mu\text{g/mL}$ (*i.e.* BSA was used as a negative control since no binding is expected for this protein). As it is shown, CR(NMe)EKA biointeracts towards the two clotted plasma proteins, being the frequency shift values higher for Fb/Fg recognition than for BSA. Moreover, provided the molecular weight of Fg and Fb is similar and *ca.* 340 kDa (Fb, which is an insoluble protein, was first dissolved in NaOH and then highly diluted in PBS), a slightly higher number of binding events occurred for Fg than Fb. As a representative example, Figure 7b depicts the nanomechanical 1st mode resonance response of a CR(NMe)EKA-functionalized Si cantilever before and after Fb incubation. The same trend was observed when Fg was used (Figure S4a), whereas BSA incubation did not lead to any significant change in the cantilever resonance frequency (Figure S4b). Although the proteins chosen play a major role in coagulation events, it is important to note that the comprehension of protein biorecognition is complex and time-demanding. CR(NMe)EKA binding towards other proteins, such as fibronectin and Fb/fibronectin mixtures are under investigation. Nevertheless, these results confirm the promising application of nanomechanical sensing to further determine the underlying binding mechanism of CREKA-based tumor-homing peptides.

Additionally, in an effort to determine the detection limit for CR(NMe)EKA, lower protein concentrations were tested in the interval between 50 ng/mL and 10 $\mu\text{g/mL}$. Figure 7c and d shows the relation between the resonance frequency shift and Fg or Fb concentration, respectively. As it can be observed, regardless the protein, the resonance frequency shift exhibits a linear dependence with the protein concentration: the higher the concentration, the more mass is being recognized by the pentapeptide, which induces greater changes in the mechanical vibration of the cantilever. Control experiments, which consisted on incubating CR(NMe)EKA-functionalized Si chips in solutions with no protein, allow us to establish a noise level produced by non-specific interactions (grey shadowed areas in Figure 7c and d). Hence, the detection limit is set at 100 ng/mL for both Fb and Fg. Despite the fact that the detection limit obtained in these measurements is above the detection range of the technique generally used to determine the concentration of Fb and Fg (*i.e.* ELISA, 0.5 - 6.25 ng/mL and 1.25 – 80 ng/mL, respectively), this label-free nanomechanical sensing offers simplicity and affordability. Furthermore, it has been proven to reach values in the order of magnitude of fg/mL by using a different configuration [34,35]. Consequently, to improve the

detection limit of the measurement, two different strategies can be applied: (i) use of smaller cantilevers; or (ii) amplify the signal by means of CREKA-functionalized nanoparticles, such as those previously described [16,20].

Bearing all these considerations in mind, this study establishes a challenging line of research focused on CREKA and CR(NMe)EKA tumor-homing peptides and their bioapplication that is currently being developed in our laboratory. Specifically, the protein recognition event if conducted in a reverse configuration, with Fb/Fg-functionalized cantilevers and PEDOT-CREKA/CR(NMe)EKA biocomposite interfaces[27,28] designed as nanoparticles [46], can significantly contribute expand the scope of nanomechanical biosensing. Moreover, in addition to tumor-homing, other functionalities of CR(NMe)EKA-based nanoparticles are aimed to be exploited in a clinical context, such as tumor imaging or drug delivery.

CONCLUSIONS

In this work, we have examined the biorecognition event between clotted plasma proteins and a tumor-homing pentapeptide, CR(NMe)EKA, by applying a label-free sensing technology based on microcantilevers. For such purpose, CREKA and CR(NMe)EKA were covalently linked *via* an epoxysilane-based protocol to Si substrates that efficiently activated by UV/ozone treatment. The results derived from the different characterization techniques performed at each one of the functionalization steps confirmed the suitability of the protocol to tether these linear, small pentapeptides onto Si surfaces. Moreover, although the presence of the NMe-Glu residue had no impact regarding the functionalization result, CR(NMe)EKA-functionalized silicon substrates yield the highest Fb adsorption in PBS in comparison to CREKA-functionalized surfaces. Hence, after the covalent binding of CR(NMe)EKA onto Si surfaces, NMe-Glu residue still promotes Fb-binding. Finally, dynamic mode nanomechanical tests were carried out using CR(NMe)EKA-functionalized microcantilever sensors. This simple and manageable label-free detection technique provided information regarding the interaction between Fb/Fg and the clot-binding peptide, thus establishing a detection limit of 100 ng/mL. However, although further improvement is required to lower the detection limit and determine the specific binding affinity of CREKA and its analogues, the overall of these results reflect the importance

of developing emerging technologies suitable for specific biomedical purposes. With that goal in mind, extensive investigation is being performed in our laboratory to comprehend CREKA and CR(NMe)EKA-mediated clot-binding and expand their applications in the biotechnological field.

ACKNOWLEDGEMENTS

This work was supported by MINECO (MAT2015-69367-R). Support for the research of C.A. was received through the prize “ICREA Academia” for excellence in research funded by the Generalitat de Catalunya. Authors gratefully acknowledge the excellent technical support received from Dr. O. Ahumada and A. Salvador-Matar (Mecwins S.L.) during nanomechanical sensing experiments and for their contribution to the results discussion. We also kindly thank Dr. M. Domínguez (Center for Research in Nano-Engineering, UPC) for technical support during XPS measurements and Dr. C. Mas-Moruno (CIBER-BBN) for his contribution to the XPS results discussion.

REFERENCES

- [1] Stewart B.W., Wild C. P. “World Cancer Report 2014,” Lyon, 2014.
- [2] Weissleder, R. Molecular imaging in cancer. *Science* 2006; **312**: 1168–1171.
- [3] Li Z.J., Cho C.H. Peptides as targeting probes against tumor vasculature for diagnosis and drug delivery. *J. Transl. Med.* 2012; **10(Suppl 1)**: S1.
- [4] Hajitou A., Pasqualini R., Arap W. Vascular targeting: recent advances and therapeutic perspectives. *Trends Cardiovasc. Med.* 2006; **16**: 80–88.
- [5] Deutscher S.L. Phage Display in Molecular Imaging and Diagnosis of Cancer. *Chem. Rev.* 2010; **110**: 3196–3211.
- [6] Li Z.J., Cho C.H. Development of Peptides as Potential Drugs for Cancer Therapy. *Curr. Pharm. Des.* 2010; **16**: 1180–1189.
- [7] Lee S., Xie J., Chen X. Peptide-Based Probes for Targeted Molecular Imaging. *Biochemistry* 2010; **49**: 1364–1376.

- [8] Arap W., Pasqualini R., Ruoslahti E. Cancer treatment by targeted drug delivery to tumor vasculature in a mouse model. *Science* 1998; **279**: 377–380.
- [9] Ellerby H.M., Arap W., Ellerby L.M., Kain R., Andrusiak R., Rio G.D., Krajewski S., Lombardo C.R., Rao R., Ruoslahti E., Bredesen D.E., Pasqualini R. Anti-cancer activity of targeted pro-apoptotic peptides. *Nat. Med.* 1999; **5**: 1032–1038.
- [10] Hood J.D., Bednarski M., Frausto R., Guccione S., Reisfeld R.A., Xiang R., Cheres D.A. Tumor regression by targeted gene delivery to the neovasculature. *Science* 2002; **296**: 2404–2407.
- [11] Sacchi A., Gasparri A., Gallo-Stampino C., Toma S., Curnis F., Corti A. Synergistic antitumor activity of cisplatin, paclitaxel, and gemcitabine with tumor vasculature-targeted tumor necrosis factor- α . *Clin. Cancer Res.* 2006; **12**: 175–182.
- [12] Lee T.-Y., Lin C.-T., Kuo S.-Y., Chang D.-K., Wu H.-C. Peptide-mediated targeting to tumor blood vessels of lung cancer for drug delivery. *Cancer Res.* 2007; **67**: 10958–10965.
- [13] Hoffman J.A., Giraudo E., Singh M., Zhang L., Inoue M., Porkka K., Hanahan D., Ruoslahti E. Progressive vascular changes in a transgenic mouse model of squamous cell carcinoma. *Cancer Cell* 2003; **4**: 383–391.
- [14] Joyce J.A., Laakkonen P., Bernasconi M., Bergers G., Ruoslahti E., Hanahan D. Stage-specific vascular markers revealed by phage display in a mouse model of pancreatic islet tumorigenesis. *Cancer Cell* 2003, **4**: 393–403.
- [15] Hatakeyama S., Sugihara K., Shibata T.K., Nakayama J., Akama T.O., Tamura N., Wong S.-M., Bobkov A.A., Takano Y., Ohyama C., Fukuda M., Fukuda M. N. Targeted drug delivery to tumor vasculature by a carbohydrate mimetic peptide. *Proc. Natl. Acad. Sci. U. S. A.* 2011, **108**: 19587–19592.
- [16] Simberg D., Duza T., Park J.H., Essler M., Pilch J., Zhang L., Derfus A.M., Yang M., Hoffman R.M., Bhatia S., Sailor M.J., Ruoslahti E. Biomimetic amplification of nanoparticle homing to tumors. *Proc. Natl. Acad. Sci.* 2007; **104**: 932–936.

- [17] Pasqualini R., Ruoslahti E. Organ targeting In vivo using phage display peptide libraries. *Nature* 1996; **380**: 364–366.
- [18] Hamzah J., Kotamraju V.R., Seo J.W., Agemy L., Fogal V., Mahakian L.M., Peters D., Roth L., Gagnon M.K.J., Ferrara K.W., Ruoslahti E. Specific penetration and accumulation of a homing peptide within atherosclerotic plaques of apolipoprotein E-deficient mice. *Proc. Natl. Acad. Sci.* 2011; **108**: 7154–7159.
- [19] Peters D., Kastantin M., Kotamraju V.R., Karmali P.P., Gujraty K., Tirrell M., Ruoslahti E. Targeting atherosclerosis by using modular, multifunctional micelles. *Proc. Natl. Acad. Sci.* 2009; **106**: 9815–9819.
- [20] Agemy L., Sugahara K.N., Kotamraju V.R., Gujraty K., Girard O.M., Kono Y., Mattrey R.F., Park J.-H., Sailor M.J., Jimenez A.I., Cativiela C., Zanut D., Sayago F.J., Alemán C., Nussinov R., Ruoslahti E. Nanoparticle-induced vascular blockade in human prostate cancer. *Blood* 2010; **116**: 2847–2856.
- [21] Kruse A.M., Meenach S.A., Anderson K.W., Hilt J.Z. Synthesis and characterization of CREKA-conjugated iron oxide nanoparticles for hyperthermia applications. *Acta Biomater.* 2014, **10**: 2622–2629.
- [22] Chung E.J., Cheng Y., Morshed R., Nord K., Han Y., Wegscheid M.L., Auffinger B., Wainwright D.A., Lesniak M.S., Tirrell M.V. Fibrin-binding, peptide amphiphile micelles for targeting glioblastoma. *Biomaterials* 2014; **35**: 1249–1256.
- [23] Stefanelli V.L., Barker T.H. The evolution of fibrin-specific targeting strategies. *J. Mater. Chem. B* 2015; **3**: 1177–1186.
- [24] Zanut D., Curcó D., Nussinov R., Alemán C. Influence of the dye presence on the conformational preferences of CREKA, a tumor homing linear pentapeptide. *Biopolymers* 2009; **92**: 83–93.
- [25] Zanut D., Flores-Ortega A., Casanovas J., Curcó D., Nussinov R., Alemán C. The Energy Landscape of a Selective Tumor-Homing Pentapeptide. *J. Phys. Chem. B* 2008; **112**: 8692–8700.
- [26] Zanut D., Sayago F.J., Revilla-López G., Ballano G., Agemy L., Kotamraju V.

- R., Jiménez A.I., Cativiela C., Nussinov R., Sawvel A.M., Stucky G., Ruoslahti E., Alemán C. Engineering strategy to improve peptide analogs: from structure-based computational design to tumor homing. *J. Comput. Aided. Mol. Des.* 2013; **27**: 31–43.
- [27] Fabregat G., Teixeira-Dias B., del Valle L.J., Armelin E., Estrany F., Alemán C. Incorporation of a Clot-Binding Peptide into Polythiophene: Properties of Composites for Biomedical Applications. *ACS Appl. Mater. Interfaces* 2014; **6**: 11940–11954.
- [28] Puiggalí-Jou A., del Valle L.J., Armelin E., Alemán C. Fibrin Association at Hybrid Biointerfaces Made of Clot-Binding Peptides and Polythiophene. *Macromol. Biosci.* **2016**; DOI: 10.1002/mabi.201600128.
- [29] Shekhawat G.S., Dravid V.P. Biosensors: Microcantilevers to lift biomolecules. *Nat. Nanotechnol.* 2015; **10**: 830–831.
- [30] Calleja M., Kosaka P.M., San Paulo Á., Tamayo J. Challenges for nanomechanical sensors in biological detection. *Nanoscale* 2012; **4**: 4925–4938.
- [31] Waggoner P.S., Craighead H.G. Micro- and nanomechanical sensors for environmental, chemical, and biological detection. *Lab Chip* 2007; **7**: 1238–1255.
- [32] Arlett J.L., Myers E.B., Roukes M.L. Comparative advantages of mechanical biosensors. *Nat. Nanotechnol.* 2011; **6**: 203–215.
- [33] Ndieyira J.W., Kappeler N., Logan S., Cooper M.A., Abell C., Mckendry R.A., Aepli G. Surface-stress sensors for rapid and ultrasensitive detection of active free drugs in human serum. *Nat. Nanotechnol.* 2014; **9**: 225–232.
- [34] Kosaka P.M., Pini V., Ruz J.J., Silva R. a da, González M.U., Ramos D., Calleja M., Tamayo J. Detection of cancer biomarkers in serum using a hybrid mechanical and optoplasmonic nanosensor. *Nat. Nanotechnol.* 2014; **9**: 1047–53.
- [35] Joo J., Kwon D., Yim C., Jeon S. Highly sensitive diagnostic assay for the detection of protein biomarkers using microresonators and multifunctional nanoparticles. *ACS Nano* 2012; **6**: 4375–4381.

- [36] Huber F., Lang H.P., Backmann N., Rimoldi D., Gerber C. Direct detection of a BRAF mutation in total RNA from melanoma cells using cantilever arrays. *Nat. Nanotechnol.* 2013; **8**: 125–129.
- [37] Wafula Ndieyira J., Watari M., Donoso Barrera A., Zhou D., Gtli M.V, Batchelor M., Cooper M.A., Strunz T., Horton M.A., Abell C., Rayment T., Aeppli, G., Mckendry R.A. Nanomechanical detection of antibiotic– mucopeptide binding in a model for superbug drug resistance. *Nat. Nanotechnol.* 2008, **3**: 691–696.
- [38] Alvarez M., Lechuga L.M. Microcantilever-based platforms as biosensing tools. *Analyst* 2010; **135**: 827–836.
- [39] Lechuga Gómez L., Álvarez-Sánchez V., Tamayo de Miguel F. J., “U.S. patent 7,646,494 B2,” 2007.
- [40] F. J. Tamayo De Miguel, J. Mertens, and M. Calleja-Gómez, “U.S. patent 7,978,344 B2,” 2011.
- [41] Ruoslahti E., Bhatia S.N., Sailor M.J. Targeting of drugs and nanoparticles to tumors. *J. Cell Biol.* 2010; **188**: 759–768., Mar. 2010.
- [42] Chevalier S., Cuestas-Ayllon C., Grazu V., Luna M., Feracci H., and De La Fuente J.M. Creating biomimetic surfaces through covalent and oriented binding of proteins. *Langmuir* 2010; **26**: 14707–14715.
- [43] Eby D.M., Artyushkova K., Paravastu A.K., Johnson G.R. Probing the molecular structure of antimicrobial peptide-mediated silica condensation using X-ray photoelectron spectroscopy. *J. Mater. Chem.* 2012; **22**: 9875–9883.
- [44] Martínez N.F., Kosaka P.M., Tamayo J., Ramírez J., Ahumada O., Mertens J., Hien T.D., Rijn C.V., Calleja M. High throughput optical readout of dense arrays of nanomechanical systems for sensing applications. *Rev. Sci. Instrum.* 2010; **81**: 125109.
- [45] Tamayo J., Pini V., Kosaka P., Martinez N.F., Ahumada O., Calleja M. Imaging the surface stress and vibration modes of a microcantilever by laser beam deflection microscopy. *Nanotechnology* 2012; **23**: 315501.
- [46] Han M.G., Foulger S.H. Crystalline Colloidal Arrays Composed of Poly(3,4-

ethylenedioxythiophene)-Coated Polystyrene Particles with a Stop Band in the Visible Regime. *Adv. Mater.* 2004; **16**: 231–234.

CAPTIONS TO FIGURES

Scheme 1. Tumor-homing peptides used in this work: CREKA and CR(NMe)EKA.

Figure 1. Experimental set-up for the nanomechanical biosensing tests.

Figure 2. Functionalization protocol of silicon surfaces with CREKA or CR(NMe)EKA pentapeptides.

Figure 3. (a) Contact angle (CA) values of water and (b) roughness (Rq) of the silicon square surface in each different step of the functionalization process. Greek letters are assigned to statistically significant different groups (p -value < 0.05).

Figure 4. N 1s high-resolution XPS spectra for each silicon surface throughout the functionalization protocol. Peaks from deconvolution are also displayed.

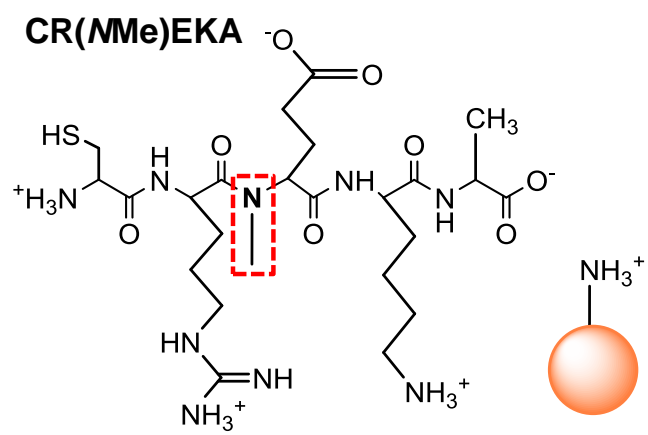
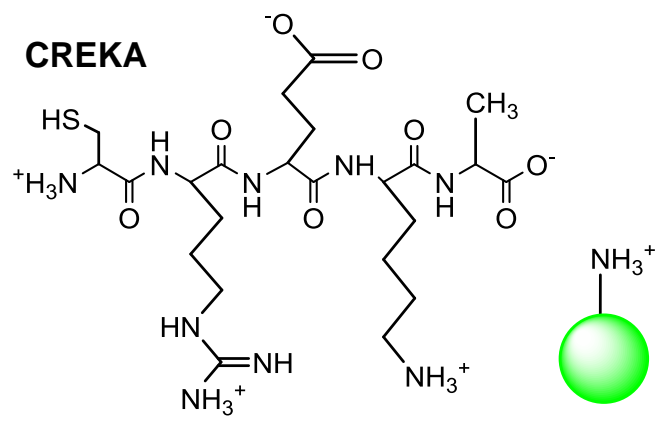
Figure 5. Topographical characterization (areas of $5 \times 5 \mu\text{m}^2$): a) 2D AFM height and b) phase micrographs of Si–OH (left) and CR(NMe)EKA (right) surfaces. c) Height profile of a horizontal line drawn as depicted in a).

Figure 6. Protein adhesion assay carried out in PBS. Absorbance values were obtained from ab-HRP activity. Greek letters on the columns refer to significant differences (p -value < 0.05) when the 2-way ANOVA and Tukey's multiple comparisons test are applied: α vs Si-CR(NMe)EKA BSA absorbance, β vs Fb absorbance on TCP.

Figure 7. Nanomechanical response: (a) absolute frequency shift of cantilevers after being incubated with $10 \mu\text{g/mL}$ of BSA, Fg and Fb; (b) mechanical resonance frequency of a Si cantilever before and after the Fb recognition event ($10 \mu\text{g/mL}$ in PBS); (c and d) relative resonance-frequency shift vs protein concentration of (c) Fg and (d) Fb in PBS. Mean values and standard deviations are calculated with the data of a minimum of 10 different cantilevers. Lines are a guide for the eye.

Table 1. Atomic percentage composition and N/C, N/O and N/Si atomic ratio for Si surfaces throughout each step of the functionalization protocol.

	O 1s	C 1s	Si 2p	N 1s	N/C	O/C	N/Si
Si-OH	47.7	13.4	38.9	-	-	3.56	-
Epoxy silane	40.1	23.5	36.4	-	-	1.71	-
TLC	36.2	24.8	39.1	-	-	1.46	-
CREKA	32.1	34.8	31.1	2.0	0.06	0.92	0.06
CR(NMe)EKA	36.7	29.6	31.4	2.3	0.08	1.24	0.07



Scheme 1

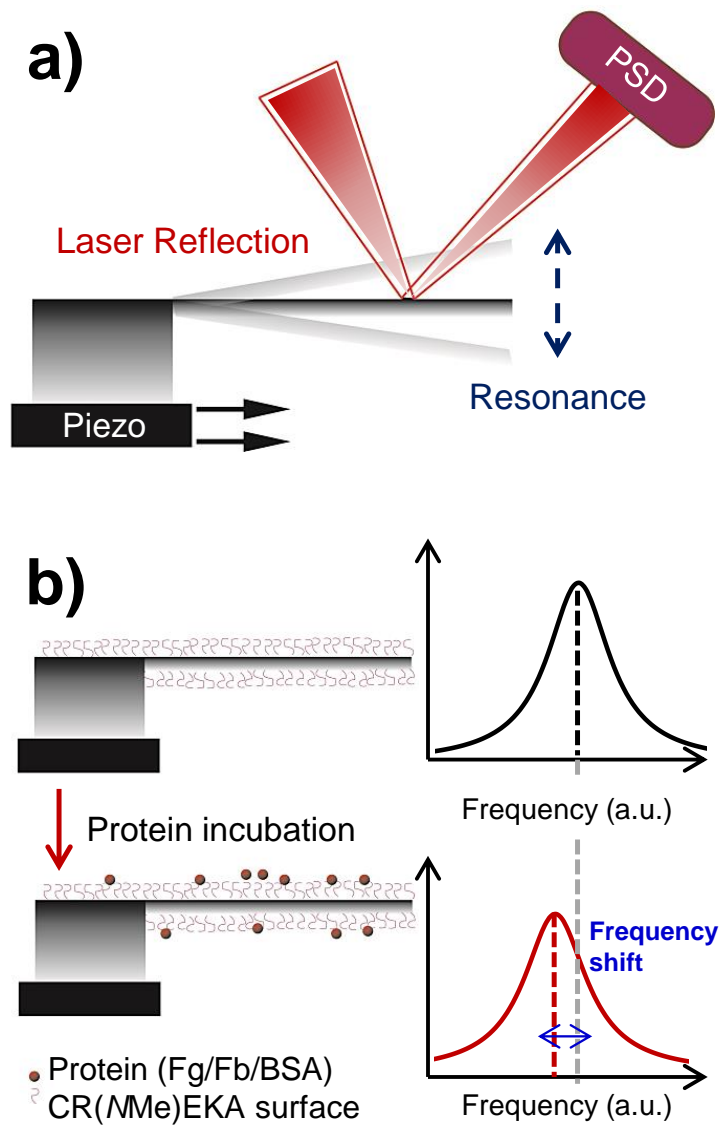


Figure 1

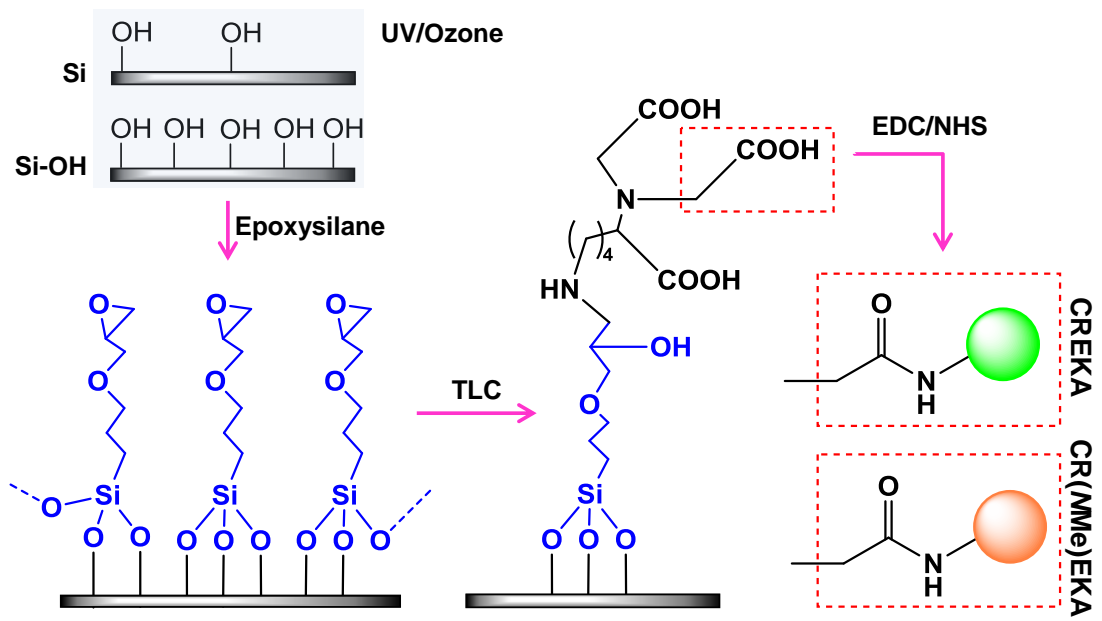


Figure 2

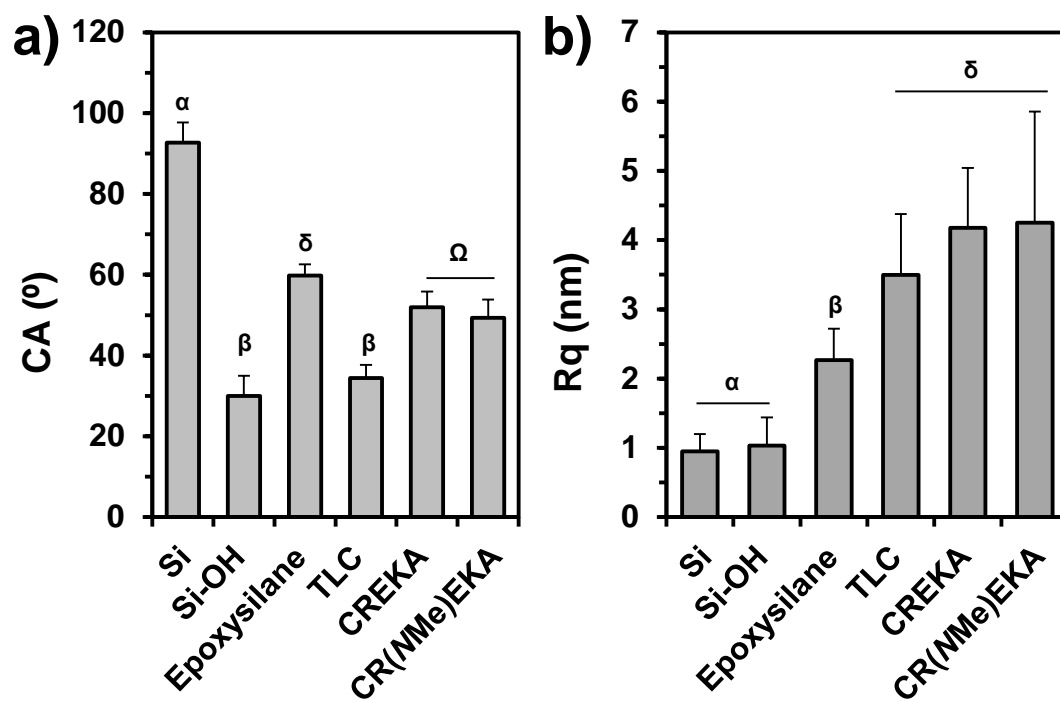


Figure 3

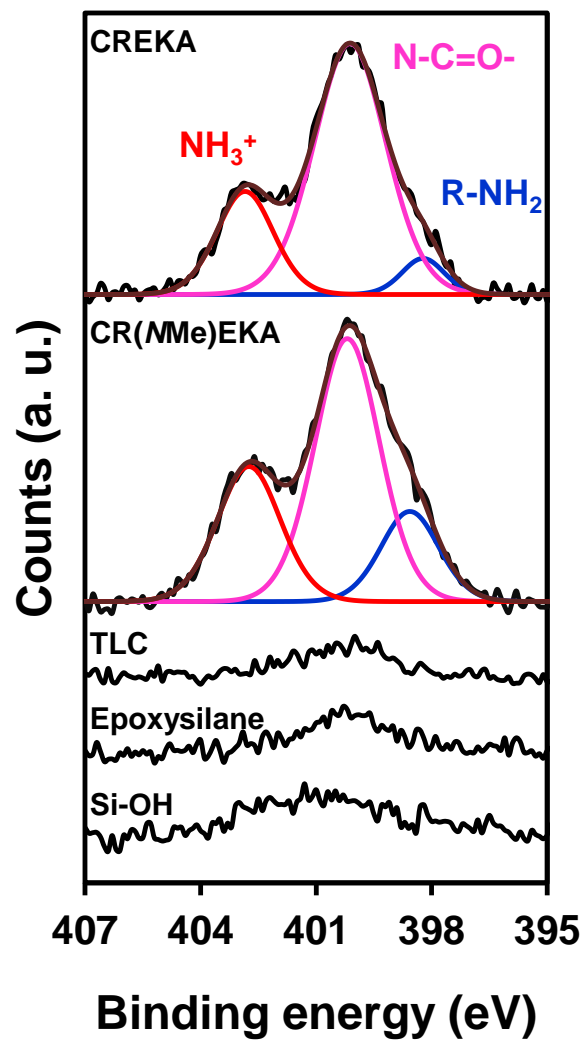


Figure 4

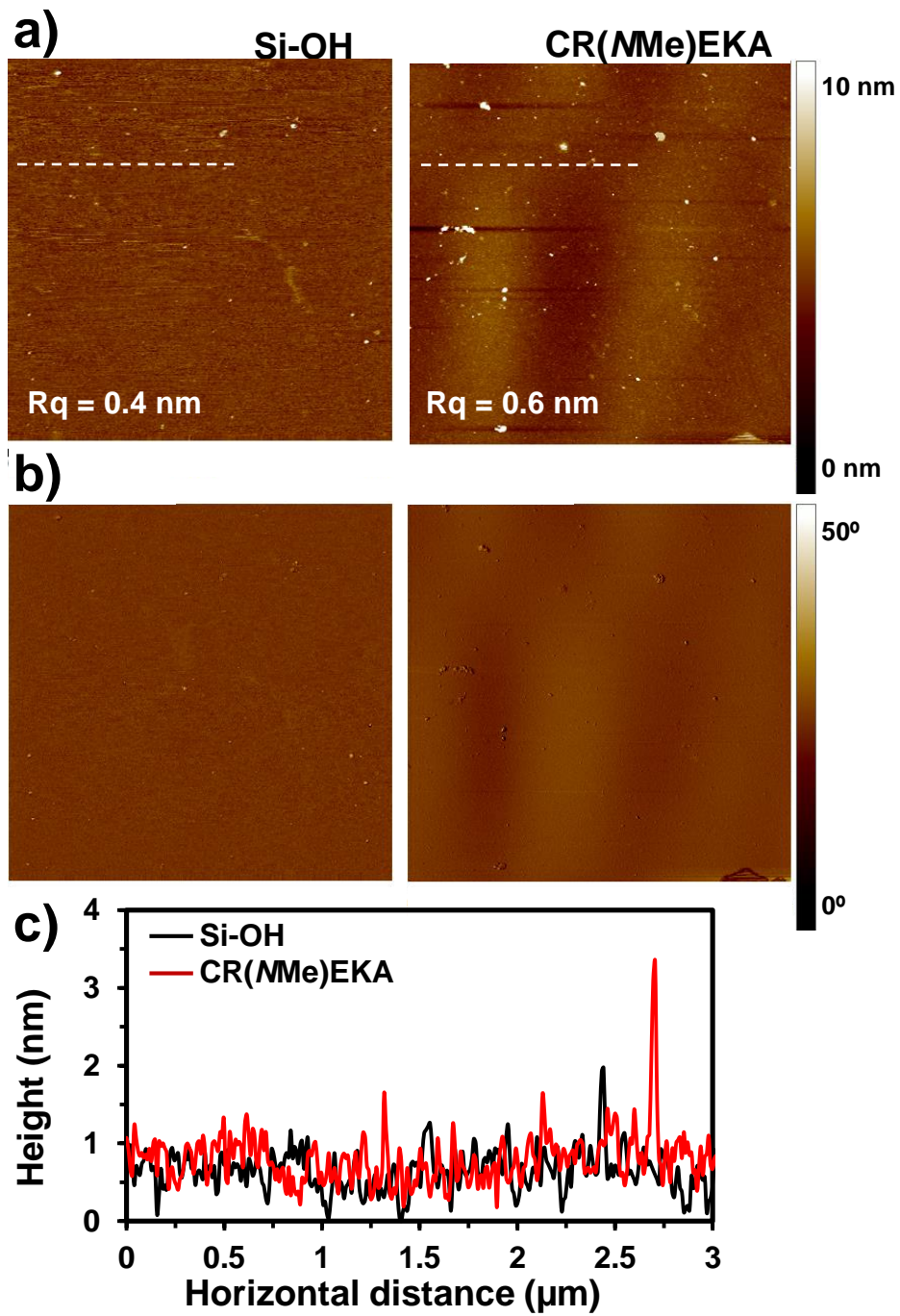


Figure 5

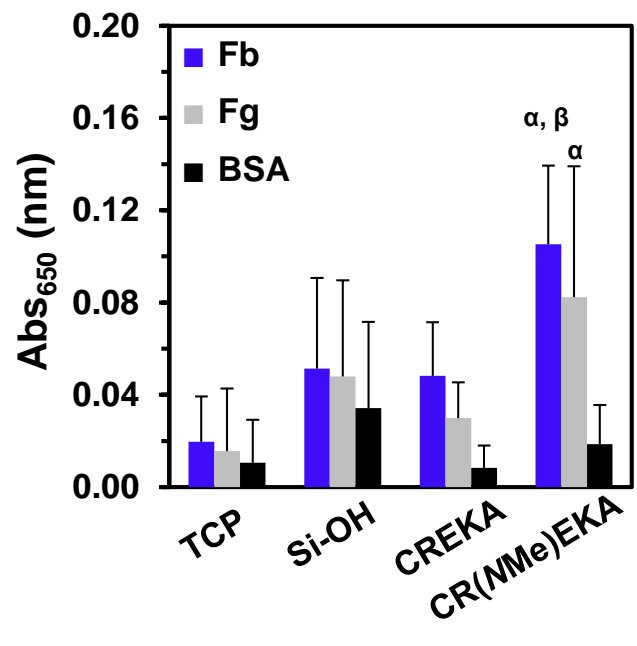


Figure 6

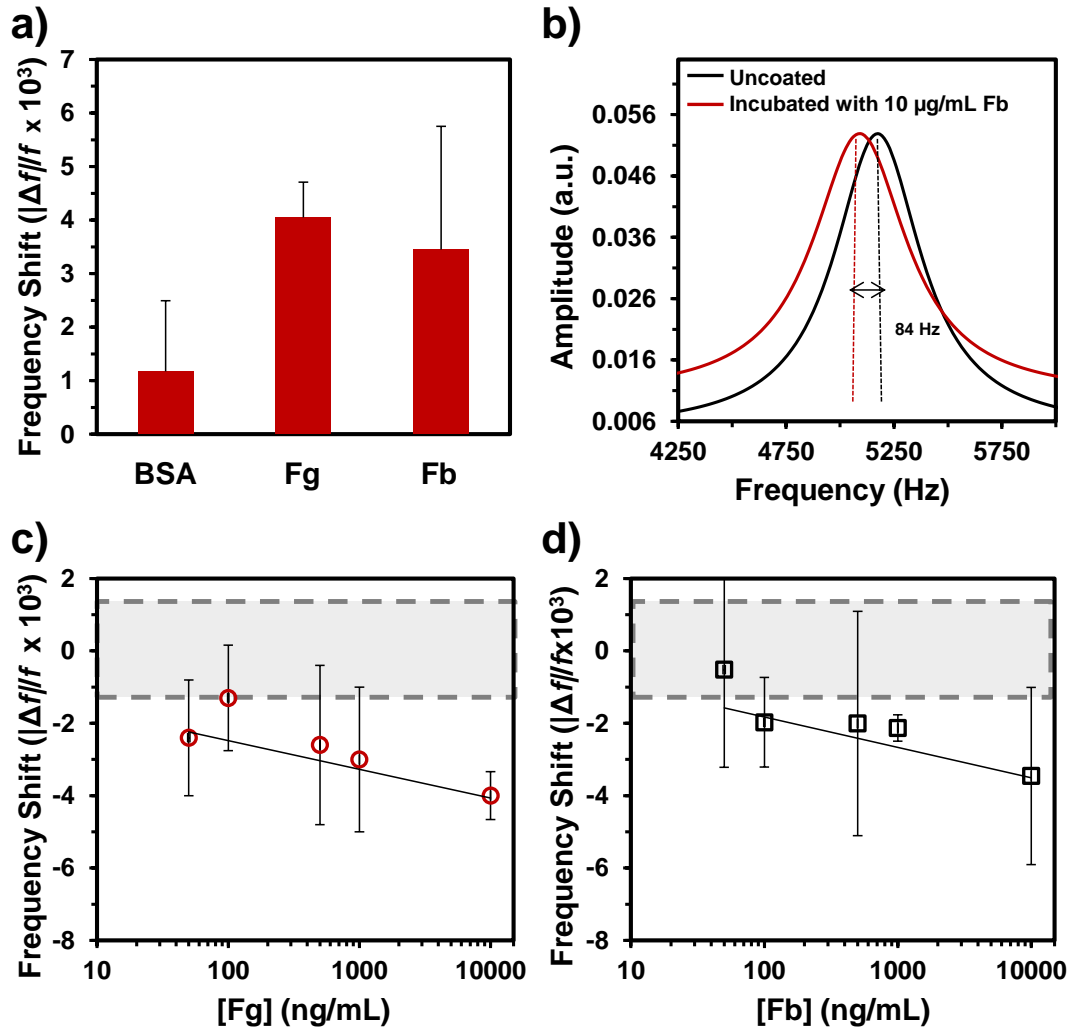


Figure 7

